CrystEngComm

Accepted Manuscript

ROYAL SOCIETY OF CHEMISTRY

www.rsc.org/crystengcomm

Cite this: DOI: 10.1039/c0xx00000x

www.rsc.org/xxxxxx

ARTICLE TYPE

Synthesis of single crystalline sub-micron rutile TiO_2 rods using hydrothermal treatment in acidic media

Patrick Leidich, Olga Linker, Martin Panthöfer, and Wolfgang Tremel*

Received (in XXX, XXX) Xth XXXXXXXXX 20XX, Accepted Xth XXXXXXXXX 20XX

DOI: 10.1039/b000000x

Size engineered rutile sub-micron rods were obtained from nanostructured titania under acidic conditions. The synthesis was performed by hydrothermal treatment starting from TiO_2-P25 and HCl. The synthesis proceeds in less than two hours and can be upscaled to several grams in a one-pot reaction by increasing the reaction time. The product is single-phase, and the particles are single crystalline as confirmed by electron diffraction and powder X-ray diffraction analysis. The length of the particles can be varied over a wide range from 100 nm to 1.3 µm by changing the acid concentration. Particle growth is proposed to proceed by a dissolution-recrystallization process via soluble $[TiCl_6]^{2-}$ or partially hydrated/hydroxylated species.

Introduction

Titanium dioxide, TiO_2, is one of the most widely used metal oxides with a broad range of applications including bioseparation,[1] sensors,[2] energy storage,[3] solar cells,[4,5] catalysis and photocatalysis.[6,7] It is abundant and cheap, chemically stable and non-toxic, while having a relatively high photocatalytic activity. Therefore, TiO_2 has been studied intensively and used as a photocatalyst in both, fundamental research and practical applications,[3,8-12] such as coatings for self-cleaning surfaces,[13,14] as photocatalyst for water splitting,[6,7,11,13] and as photoanodes in dye-sensitized solar cells.[4,5,13,14]

TiO_2 is polymorph, exhibiting the crystal structures of rutile, anatase, and brookite. Rutile is the only stable phase in the phase diagram. Anatase and brookite are metastable, yet. Banfield and co-workers[15-17] investigated the phase stability of TiO_2 as a function of its particle size and demonstrated that rutile as a bulk material is more stable than anatase, whereas a crossover in stability to anatase occurs for particle sizes smaller than 14 nm due to the surface energy contribution.[15-18] Furthermore, initial size effects are crucial for the transformation behavior of a mixture of anatase (5.1 nm) and brookite particles (8.1 nm). In a first step, anatase transforms to brookite and/or rutile, and eventually single-phase rutile is formed.[19] Wet chemical preparation methods for TiO_2 generally favor the formation of anatase.[19-22] Therefore, anatase nanoparticles can easily be made. Brookite is more difficult to synthesize, therefore, it has no important industrial applications so far.

Structural stability is typically rationalized based on a molecular picture, where the nucleation and growth of the different TiO_2 polymorphs are determined by the precursor chemistry, i.e. the reactants.[23–29] However, the kinetics of particle formation is related to the broad variety of experimental conditions used for the synthesis of the different TiO_2 phases, which makes a comparison of formation mechanisms difficult.

The materials properties of TiO_2 nanoparticles are a function of crystal structure, nanoparticle size, and morphology, and, therefore, strongly dependent on the method of synthesis.[20,21,30-32] Wet chemical approaches use high boiling organic solvents with detergents, such as SDS and CTAB, to acquire control over size and morphology. Anatase nanoparticles have been made from aqueous solution starting from titanium alkoxide precursors, where single phase anatase nanoparticles with diameters ranging from 6–30 nm were formed under acidic and basic conditions.[33] In strong acids the product usually contained a large fraction of brookite nanoparticles.[34,35] Larger anatase particles are difficult to prepare because of the phase transformation to rutile due to the surface to bulk energy ratio. Single-phase brookite particles (0.3–1 µm) have been prepared by hydrothermal treatment of amorphous titania in NaOH.[36] The mechanism is related to the formation of sodium titanate,[37-44] which subsequently transforms to TiO_2. Brookite nanoparticles in the size range of 5–10 nm were obtained by thermolysis of $TiCl_4$ in aqueous HCl,[29] where the phase composition of the reaction product was dependent on the Ti/Cl ratio. Phase mixtures with a brookite content of 80% could be obtained for Ti/Cl ratios of 17-35. The brookite nanoparticles could be separated by selective precipitation of rutile. For higher Ti/Cl ratios, pure rutile particles were obtained. Phase-pure rutile nanoparticles have been prepared from $TiCl_4$ or $TiCl_3$ in HCl or from titanium isopropoxide in nitric acid.[26,27,45,46] Recently, synthesis methods for the three phases have been compared to determine the effect of crystal structure on the physical properties.[28,47] An understanding of the key parameters that determine phase selection and crystal growth is crucial for a successful technological application of TiO_2.

Here, we present a fast and facile one-pot synthesis of rutile submicron rods using a microwave-assisted hydrothermal treatment procedure. These particles are single crystalline; moreover, it was also possible to tune the length of the rods by adjusting the acid concentration. The approach using a microwave-assisted hydrothermal treatment was utilized to gain insight into the growth of the rutile rods, to identify the driving force behind their formation

and to propose a plausible reaction mechanism. Compared to conventional hydrothermal reactions in stainless steel autoclaves, microwave-assisted reactions offer several advantages, such as rapid heating due to a direct response of the solvent to microwaves and short cooling cycles due to the lower heat capacity of the reaction vessel. Owing to the fast cooling time, it is possible to quench the reaction to take "snapshots" of the reaction intermediates by an *ex-situ* structural investigation in order to gain mechanistic (i.e. morphological, chemical and crystallographic) information. Another advantage of the microwave-assisted reaction are short reaction times of 1-2 h[44,48] compared to conventional hydrothermal reactions that require typically 24 h or more.[37-42,49-51] The resulting sub-micron rutile rods are suitable for various applications such as photocatalysis and electrodes for dye-sensitized solar cells.

Experimental

Materials. All materials were used as received without any further purification. TiO_2-P25 nanoparticles were purchased from Degussa. Aqueous HCl solutions of various concentrations were made by dilution of conc. HCl (≥37%, Fluka, analytical grade) with MilliQ-water (18.2 MΩ/cm). Ethanol (p.A.) was purchased from VWR. HBr (48% aqueous solution) and HI (57% aqueous solution with 1.5% hypophosphoric acid) were purchased from ABCR.

Synthesis. The microwave-assisted hydrothermal treatment was carried out using a MARS5 digestion system (CEM Corporation), equipped with XP1500 high pressure vessels and pressure control. The reaction was also carried out in stainless steel autoclaves with 50 mL Teflon inlays (Berghoff Corporation). In a standard reaction, 500 mg TiO_2-P25 were mixed with 6 M HCl (10 mL MilliQ-water and 10 mL of conc. HCl). For a synthesis in a microwave-assisted reaction system, the mixture was ramped up to 30 bar over 10 min with a maximal power of 1600 W, and held at 30 bar for 90 min. After the reaction was completed, it was cooled down to room temperature over 30 min. Alternatively, the reaction was carried out in a stainless steel autoclave for 12 h at a temperature of 220°C, and cooled down afterwards. The reaction mixture was centrifuged, the supernatant was discarded, and the solid was rinsed repeatedly with water and ethanol until the solution was neutral. Afterwards, the residue was dried overnight at 70°C.

Characterization

Electron microscopy. Sub-micron TiO_2 rods were characterized by (high angle annular dark field) transmission electron microscopy (HAADF TEM) and low-resolution transmission electron microscopy (TEM). A Philips EM 420 instrument with an acceleration voltage of 120 kV and LaB_6 cathode was used for low-resolution TEM images. HAADF TEM images and electron diffraction patterns were recorded with a HR FEI Tecnai F30 S-Twin using an accelerating voltage of 300 kV with a field emission gun. For preparation, the samples were dispersed in ethanol and dropped on a carbon-coated copper grid.

X-ray diffraction. X-ray diffraction patterns were recorded using a Siemens D5000 diffractometer equipped with a Braun M50 position sensitive detector in transmission mode using Ge (200) monochromatized CuK_α radiation. Crystalline phases were identified according to the PDF-2database. Diffraction data were modeled by Rietveld refinements using TOPAS Academic V5 applying the fundamental parameter approach.[52,53]

Results and Discussion

Crystal phase evolution

Our study was conducted by fast hydrothermal treatment in a microwave-assisted pressurized vessel. For instance, 500 mg of single crystalline sub-micron rutile rods were produced easily in 90 min, and higher yields are easily achievable by extending the reaction time, with no further adjustments necessary. A 4-hour reaction, for example, yields 5 g of product. All reactions we refer to in the following yielded 500 mg of product, as reaction times and velocities are dependent on the yield of the reaction.

The powder X-ray diffraction (PXRD) patterns in Figure 1a show that after 90 min reaction time, subsequent to 10 min ramping up to a pressure of 30 bar, rutile is the only crystalline phase with minor impurities of anatase (<3 (5) wt%) according to the PXRD pattern. The crystallite sizes of the rutile phase were determined as 221 (6) nm in length and 112 (1) nm in width.

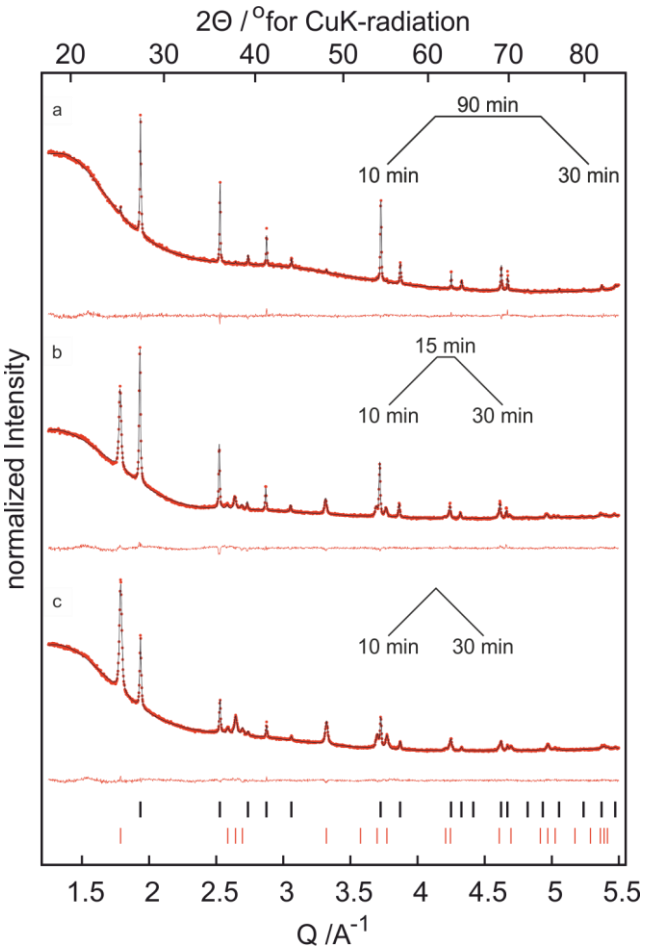

Figure 1. Rietveld refinement (black line) of the X-ray powder diffraction data (red dots) and residuum (red line) for samples obtained after hydrothermal treatment of TiO_2-P25 after a) 90 min, b) 15 min, and c) 0 min heating time subsequent to 10 min ramping time to a pressure of 30 bar. The black and red ticks mark the reflections for rutile and anatase, respectively. Graphical insets show the heating profiles.

We took "snapshots" (by fast quenching) of the reaction at different stages. The starting material TiO_2-P25 was a mixture of anatase and rutile (see Figure S1). The time frame of the reaction was determined to 90 min by quenching the reaction at different reaction durations and set to the point of time when no precursor was detectable any more by X-ray diffraction and TEM. The phase composition and the crystallite sizes of the reaction products and intermediates were determined by Rietveld refinements.

X-ray powder diffraction patterns of reaction intermediates taken after time intervals of 0 and 15 min show that the precursor material was depleted during the reaction, as indicated by the vanishing fraction of anatase, in agreement with the results of the TEM analysis (TEM snapshots in Figure S2a,b). Figure 1 shows Rietveld refinements of PXRD data of the reaction stopped after different reaction times. A comparison of the data of the reaction interrupted directly (Figure 1c) after ramping to 30 bar as well as after 15 min (Figure 1b) to the data of a completed reaction after 90 min (Figure 1a) clearly shows that no precursor remains as confirmed via TEM. At the beginning of the reaction (directly after the ramping), the mixture contained 36 (1) wt% rutile with a crystallite size of 84 (1) nm. Within the first 15 min of the reaction, the rutile fraction increased to 60 (2) wt%. After 90 min, the transformation to rutile was virtually complete (96 (5) wt%, crystallite size 196 (45) nm) with traces of anatase (3.5 (5) wt%). Longer reaction times did not lead to changes in phase composition (based on X-ray data), but showed particle growth via aggregated alignment (Figure 2c + d).

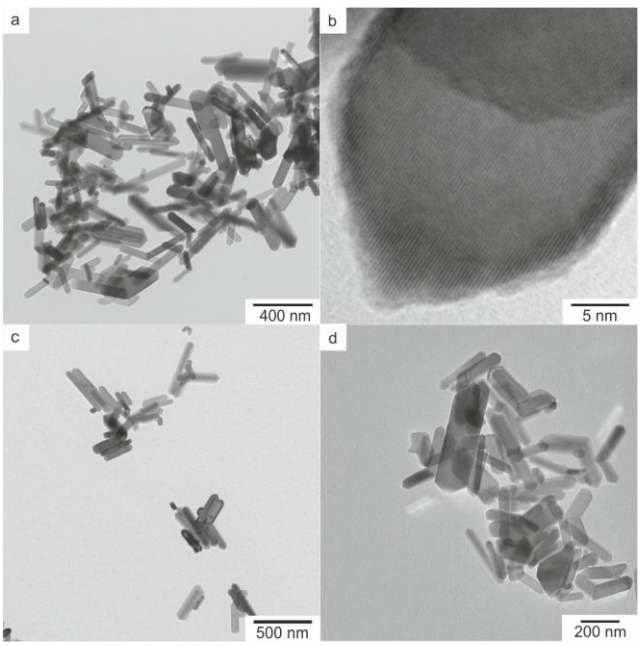

Figure 2. TEM-images of sub-micron rutile rods. a) Overview after 90 min reaction time using 6 M HCl and microwave-assisted hydrothermal treatment, b) close-up image of a tip, c) alternative reaction route using 6 M HCl and steel autoclaves, treatment duration 12 h, the particles show already alignment next to each other along their long axis, and d) also using the alternative reaction route via a steel autoclave, 6 M HCl and 24 h reaction time, showing coalescence of particles (bottom right)

Particle size and morphology

During the reaction, the size and morphology of the rods changed in a systematic manner: TEM images of the reaction product (Figure 2) show the formation of faceted particles with lengths ranging from 100 to 400 nm. The average length of the particles fits well to that determined by XRD. The polydispersity of the particles indicates that nucleation occurs continuously during the reaction. All particles have a uniform shape; a regular growth of contact twins was observed, the contact angles of all twins being identical.

The concentration of the acid has a large effect on the size distribution of the resulting particles: As the rods are not monodisperse, the size range is given in the sequel. For a reaction of 90 min in 6 M HCl sub-micron rods with lengths ranging from 100 to 400 nm were formed (Figure 3b). With decreasing HCl concentration the length of the rods decreases, the reaction rate decreases, and - as a result - the reaction time increases. In 3 M HCl the particle length dropped to 80 - 150 nm (Figure 3a), whereas 12 M HCl (conc.) yielded particles with lengths up to 500 nm to 1.3 µm (Figure 3c). However, the particles shown in this image do not exhibit well-defined facets.

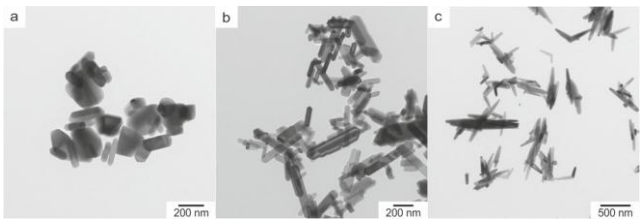

Figure 3. TEM images of TiO_2 rods of different lengths controlled by varied acid concentrations: a) 80 - 120 nm rods using 3 M HCl, b) 100 - 400 nm using 6 M HCl, and c) 500 nm – 1.3µm using conc. HCl (12 M).

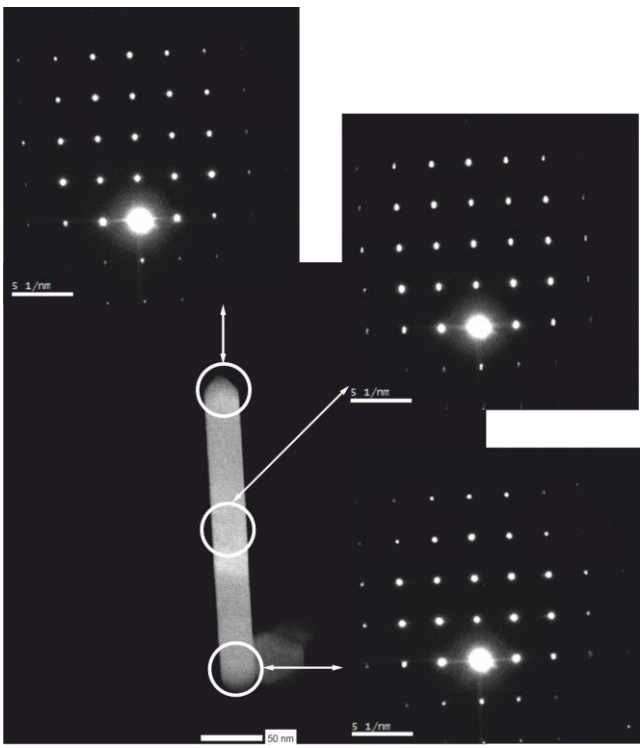

Figure 4. HAADF TEM image of a sub-micron TiO_2 rod (bottom left) and nano-electron diffraction of the shaft (top right) and both tips of the rod (top left, bottom right).

Figure 4 shows a close up HAADF TEM image of a sub-micron TiO_2 rod. Clear facets could be identified. The rod is single crys-

talline, as demonstrated by nano-electron diffraction at the shaft and both tips of the rod. The growth direction of the rod could be determined to be [110] by measuring the distance in between the lattice planes.

Growth mechanism model

The TEM images in Figure 2c and d show particles after a complete reaction (90 min microwave hydrothermal treatment or 12 h using a steel autoclave, respectively) and after a double reaction time (180 min or 24 h, respectively). It appears that rods, after the precursor was consumed, coalign (Figure 2c) and merge (Figure 2d) with time in the reaction medium. However, the pathway by which oriented attachment occurs is difficult to establish. Although the preservation of primary particle morphology and the formation of twins and stacking faults at particle-particle boundaries strongly suggest a sequence of whole-particle alignment followed by interface elimination,[26,54] atom-by-atom reorientation via dislocation and grain-boundary migration after attachment may be another potential mechanism.[55]

In order to elucidate the driving forces behind the growth process we varied the reaction parameters. (i) When HCl was replaced by sulfuric acid, phosphoric or nitric acid with adjusted Cl^- concentrations, no TiO_2 rutile rods were formed. A possible reason for this could be that these other acids do not aid the dissolution of the TiO_2-P25 precursor. Additionally, it was shown by Wu *et al*.[35] that in H_2SO_4 anatase grows preferentially due to the strong stabilization of the positively charged TiO_2 surface by SO_4^{2-}, whereas weakly coordination NO_3^- does not lead to a preference in crystal growth. In a similar manner HCl is assumed to facilitate the formation of rutile. Performing a hydrothermal treatment in pH neutral media with adjusted Cl^- concentration did not lead to any change in phase or morphology, whereas using NaOH can lead to the formation of anatase or sodium titanates depending on the experimental conditions.[37,44,56] (ii) In contrast, when the reactions were carried out in HBr and HI (Figure S3a,b), sub-micron rutile rods were formed in an analogous manner. This indicates that $[TiX_6]^{2-}$ halogentitanate-anions (X= Cl^-, Br^-, I^-) or related hydrated/hydroxylated species could be involved as intermediates in a dissolution and growth transport mechanism.[57] Surprisingly, we did not observe the growth of rutile rods in HF or NH_4F solution. We assume that in the various reactions either the fluoride concentration was too low for TiF_6^{2-} to form or that the solubility of the hexafluoro anion in the acidic solution was too high to allow a "chemical transport reaction" to proceed. HCl, HBr, or HI seems to act as mineralizers that aid the solubilization of the nutrient solid and, thereby, facilitate the transport of the insoluble TiO_2 "nutrient" to a seed crystal via a reversible transport reaction. Over time, the seed nanocrystals accumulate the material that was before in the nutrient and, therefore, keep growing. Many hydrothermal reactions involve the crystallization of solids as the properties of solvents under subcritical conditions may undergo dramatic changes.[58,59] Attempts to demonstrate the presence of intermediate species by Raman, infrared (IR) or as UV-VIS spectroscopy were not successful. We was also attempted to crystallize the intermediate species by adding sterically demanding cations, but without effect. *In situ* measurements (pH=0, 30 bar) might be useful in this respect, because the growth of rutile rods starting from TiO_2-P25 in boiling HCl under normal pressure was not possible and no intermediate (that could have been extracted) was present.

Starting from soluble precursors like $TiCl_4$ and $Ti(OBu)_4$ enables the formation of anisotropic rutile particles at lower temperatures, starting at 40°C.[60,61,46] Such reactions were performed under normal conditions and enable the possibility of *in situ* measurements. Starting from soluble Ti precursors Yin *et al*. proposed a growth via $[Ti(OH)_nCl_{6-n}]^{2-}$ anions (*n* increasing with HCl concentration).[27] The hydrolysis of $TiCl_4$ at 40-70°C in aqueous HCl to $[Ti(OH)_nCl_{6-n}]^{2-}$ might explain why intermediate species could not be detected.[27,46,60,61] Based on chemical analogy of Ti^{4+} and Sn^{4+} we attempted the growth of SnO_2 nanorods, where the corresponding (more stable) $[SnCl_6]^{2-}$ intermediates could in fact be demonstrated by precipitation with a sterically demanding (and weakly interacting) tetraphenylphosphonium cation. The x-ray diffraction pattern of this chlorostannate intermediate is shown in Figure S4. The x-ray diffraction pattern exhibits a large number of reflections due to the presence of several different chlorostannates. Yet, the most prominent reflections of $(Ph)_4P[SnCl_5(H_2O)]$ are clearly observed as shown by a Pawley fit based on the available structure data.[62] This finding supports the hypothesis that chlorotitanate intermediates play a critical role in the growth of TiO_2 nanocrystals (as proposed by Yin *et al*.[27]). The advantage of TiO_2-P25 or colloidal rutile[63,64] (rather than from rather than from humidity-sensitive and costly soluble Ti precursors) is that it is stable and inexpensive. Therefore other solid precursors (pure anatase and rutile) were tested to identify the driving force behind the formation of the rods. Bulk precursors (micron-sized particles) did not show any reactivity, presumably because their lattice energy was too high. Rutile nanoparticles (⊘ ≈ 30 nm), obtained from TiO_2-P25 by ball milling, did not show a significant reactivity either, whereas anatase nanoparticles (⊘ ≈ 15 nm) easily transformed to rutile. Calculations by Curtiss and Banard[60] revealed a crossover of the thermodynamic stability for TiO_2 caused by different surface and crystallization energies for rutile and anatase. Below a critical size, anatase becomes more stable than rutile due to its lower surface energy. The surface energy is highly dependent on the surrounding medium as demonstrated by the formation of rutile nanorods in the presence of 3-hydroxytyramine ligands.[65,66] For hydrogen-rich surfaces, Banard and Curtiss[60] calculated the crossover at a particle size of 18.4 nm at ambient temperature. The critical size, however, decreases dramatically with increasing temperature. This finding may explain the lack in reactivity of well-crystallized rutile nanoparticles under strongly acidic conditions: Rutile is the most stable phase. In contrast, the stability of anatase decreases with increasing temperature. As a result, the transformation to rutile rods becomes favorable. Banard and Curtiss[60] also rationalize the different reactivity of the nanoparticular precursors based on their instability and subsequent dissolution. The rutile rods assemble because at high H^+ concentration the TiO_2 surfaces are positively charged,[46,61] which facilitates rutile growth.

For TiO_2-P25 we assume that the rutile particles are highly defective, and, hence, show a significant reactivity under the given experimental conditions. The combination of (i) precursor instability, (ii) surface stabilization of the product and (iii) enhanced atom mobility through the formation of soluble intermediates in

the acidic HCl medium appears to be responsible for the formation the rutile particles.

Conclusions

We have reported and mechanistically rationalized the synthesis of single crystalline sub-micron rutile rods from stable solid precursors in a microwave-assisted hydrothermal reaction. All previously reported syntheses of unfunctionalized rutile particles start from air sensitive or expensive precursors, such as titanium tetrachloride or titanium tetrabutoxide. The single crystalline rods were analyzed by PXRD and HAADF/TEM. The size of the particles may be controlled by varying the HCl concentration. The growth of sub-micron rods may be rationalized based on the interplay between the precursor instability due to size and crystallinity, atom mobility be complex formation and surface stabilization by the reaction medium, i.e. the crystallization of rutile rods was promoted by the acidic medium and the Cl^- anion. In analogy to chlorostannate intermediates observed during the formation of SnO_2 we assume soluble $[Ti(OH)_nCl_{6-n}]^{2-}$ intermediates to act as mineralizers by enhancing atom mobility at the particle surfaces.[67,68]

Acknowledgements

We are grateful to the Deutsche Forschungsgemeinschaft (DFG) for financial support from the Schwerpunktprogramm SPP1415 “Kristalline Nichtgleichgewichtsphasen”.

Notes and references

Institut für Anorganische Chemie und Analytische Chemie der Johannes Gutenberg-Universität, Duesbergweg 10-14, D-55099 Mainz, Germany
**Corresponding Author: E-Mail: tremel@uni-mainz.de*

1 S. P. Albu, A. Ghicov, J. M. Macak, R. Hahn, and P. Schmuki, *Nano Lett.*, 2007, **7**, 1286.
2 S.-J. Bao, C. M. Li, J.-F. Zang, X.-Q. Cui, Y. Qiao, and J.Guo, *Adv. Funct. Mater.*, 2008, **18**, 591.
3 D. Deng , M. G. Kim, J. Y. Lee, and J. Cho, *Energy Environ. Sci*., 2009, **2**, 818.
4 M. Stefik, F. J. Heiligtag, M. Niederberger, M. Grätzel, *ACS Nano*, 2013, **7**, 8981.
5 A. Hagfeldt, G. Boschloo, L. Sun, L. Kloo, and H. Pettersson *Chem. Rev*., 2010, **110**, 6595.
6 A. Fujishima and K. Honda, *Nature*, 1972, **238**, 37.
7 A. Kudo and Y. Miseki, *Chem. Soc. Rev*., 2009, **38**, 253.
8 H. J. Yun, H. Lee, J. B. Joo, W. Kim, and J. Yi, *J. Phys. Chem. C*, 2009, **113**, 3050.
9 Q. Zhang, D. Q. Lima, I. Lee, F. Zaera, M. Chi, and Y. Yin, *Angew. Chem. Int. Ed.*, 2011, **50**, 7088.
10 H. Chen, C. E. Nanayakkara, and V. H. Grassian, *Chem. Rev*., 2012, **112**, 5919.
11 K. Nakata and A. Fujishima, *J. Photochem. Photobiology C: Photochem. Rev.*, 2012, **13**, 169.
12 T. Yuranova, R. Mosteo, J. Bandara, D. Laub, and J. Kiwi *J. Mol. Catal. A*: *Chemical*, 2006, **244**, 160.
13 T. Kamegawa, Y. Shimizu, and H. Yamashita, *Adv. Mater*., 2012, **24**, 3697.
14 N. Tetreault, E. Arsenault, L.-P. Heiniger, N. Soheilnia, J. Brillet, T. Moehl, S. Zakeeruddin, G. A. Ozin, and M. Grätzel, *Nano Lett*., 2011, **11**, 4579.
15 A. A. Gribb and J. F. Banfield, *Am. Mineral*., 1997, **82**, 717-728.
16 M. R. Ranade, A. Navrotsky, H. Z. Zhang, J. F. Banfield, S. H. Elder, A. Zaban, P. H. Borse, S. K. Kulkarni, G. S. Doran, and H. J. Whitfield, *Proc. Natl. Acad. Sci. U. S. A.*, 2002, **99**, 6476.
17 H. Z. Zhang and J. F. Banfield, *J. Mater. Chem*., 1998, **8**, 2073.
18 H. Z. Zhang and J. F. Banfield, *J. Phys. Chem., B* 2000, **104**, 3481.
19 A. Navrotsky, *Geochem. Trans*., 2003, **4**, 34.
20 C. J. Barbe, F. Arendse, P. Comte, M. Jirousek, F. Lenzmann, V. Shklover, and M. Grätzel, *J. Am. Ceram. Soc*., 1997, **80,** 3157.
21 R. L. Penn and J. F. Banfield, *Geochim. Cosmochim. Acta*, 1999, **63**, 1549.
22 M. P. Finnegan, H. Zhang, and J. F. Banfield, *J. Phys. Chem. C*., 2007, **111**, 1962.
23 H. Cheng, J. Ma, Z. Zhao, and L. Qi, *Chem. Mater*., 1995, **7**, 663.
24 K. Yanagisawa, Y. Yamamoto, Q. Feng, and N. Yamasaki, *J. Mater. Res.*, 1998, **13**, 825.
25 K. Yanagisawa and J. Ovenstone, *J. Phys. Chem. B*, 1999, **103**, 7781.
26 S. T. Aruna, S. Tirosh, and A. Zaban, *J. Mater. Chem*., 2000, **10**, 2388.
27 H. Yin, Y. Wada, T. Kitamura, S. Kambe, S. Murasawa, H. Mori, T. Sakata, and S. Yanagida, *J. Mater. Chem.*, 2001, **11**, 1694.
28 J. G. Li, T. Ishigaki, and X. Sun, *J. Phys. Chem., C* 2007, **111**, 4969.
29 A. Pottier, C. Chaneac, E. Tronc, L. Mazerolles, and J.-P. Jolivet, *J. Mater. Chem.*, 2001, **11**, 1116.
30 E. Matijevic, *Langmuir*, 1986, **2**, 12.
31 T. Sugimoto, *Adv. Colloid Interface Sci*., 1987, **28**, 65.
32 J. Livage, M. Henry, and C. Sanchez, *Prog. Solid State Chem*., 1988, **18**, 259.
33 A. Zaban, S. T. Aruna, B. A. Tirosh, B. A. Gregg, and Y. Mastai, *J. Phys. Chem. B*, 2000, **104**, 4130.
34 G. Oskam, A. Nellore, R. L. Penn, and P. Searson, *J. Phys. Chem. B*, 2003, **107**, 1734.
35 M. Wu, G. Lin, D. Chen, G. Wang, D. He, S. Feng, and R. Xu, *Chem. Mater.*, 2002, **14**, 1974.
36 T. Nagase, T. Ebina, T. Iwasaki, H. Hayashi, Y. Onodera, and M. Chatterjee, *Chem. Lett*., 1999, **9**, 911.
37 T. Kasuga, M. Hiramatsu, A. Hoson, T. Sekino, and K. Niihara, *Adv. Mater*., 1999, **11**, 1307.
38 Q. Chen, G. H. Du, S. Zhang, and L. Peng, *Acta Crystallogr, Sect. B: Struct. Sci.*, 2002, **58**, 587.
39 J. J. Yang, Z. Jin, X. Wang, W. Li, J. Zhang, S. Zhang, X. Guo, and Z. Zhang, *Dalton Trans*., 2003, 3898.
40 R. Z. Ma, Y. Bando, and T. Sasaki, *Chem. Phys. Lett*., 2003, **380**, 577.
41 S. Zhang, Q. Chen, and L. M. Peng, *Phys. Rev. B, 2005*, **71**, 014104.
42 A. Gloter, C. Ewels, P. Umek, D. Arcon, and C. Colliex, *Phys. Rev. B*, 2009, **80**, 035413.
43 I. Andrusenko, E. Mugnaioli, T. Gorelik, D. Koll, M. Panthöfer, W. Tremel, and U. Kolb, *Acta Crystallogr. Sect. B*, 2011, **67**, 218.
44 D. Koll, I. Andrusenko, E. Mugnaioli, M. Panthöfer, U. Kolb, and W. Tremel, *Z. Anorg. Allg. Chem.*, 2013, **639**, 2521.
45 C. C. Wang and J. Y. Ying, *Chem. Mater.*, 1999, **11**, 3113.
46 W. Wang, B. Gu, L. Liang, W. Hamilton, and D. Wesolowski, *J. Phys. Chem. B*, 2004, **108**, 14789.
47 K. Tomita, V. Petrykin, M. Kobayashi, M. Shiro, M. Yoshimura, and M. Kakihana, *Angew. Chem. Int. Ed*., 2006, **45**, 2378.
48 A. Birkel, F. Reuter, D. Koll, S. Frank, R. Branscheid, M. Panthöfer, E. Rentschler, and W. Tremel, *CrystEngComm.*, 2011, **13**, 2487.
49 C.-W. Peng, M. Richard-Plouet, T.-Y. Ke, C.-Y. Lee, H.-T. Chiu, C. Marhic, E. Pouzenat, F. Lemoigno, and L. Brohn, *Chem. Mater*., 2008, **20**, 7228.
50 D. V. Bavykin and F. C. Walsh, *Eur. J. Inorg. Chem.*, 2009, 977.
51 Y. W. L. Lim, Y. Tang, Y. H. Cheng, and Z. Chen, *Nanoscale*, 2010, **2**, 2751.
52 A. Coehlo, *TOPAS Academic*, V 5; Coehlo Software, Brisbane, Australia, **2012.**
53 R.W. Cheary and A. Coelho, *J. Appl. Cryst.*, 1992, **25**, 109.
54 R. L. Penn and J. F. Banfield, *Am. Mineral*., 1998, **83**, 1077.
55 C. W. Passchier and R. A. J. Trouw, Microtectonics, Springer, Sturtz, Wurzburg, Germany, 1998.
56 J.-N. Nian and H. Teng, *J. Phys. Chem. B*, 2006, **110**, 4193
57 M. Kakihana, M. Kobayashi, K. Tomita, and V. Petrykin, *Bull. Chem. Soc. Jpn*., 2010, **83**, 1285.
58 R. W. Shaw, B. B. Thomas, A. C. Antony, A. E. Charles, and E. U. Franck, *Chem. Eng. New*., 1991, Dec. 23,26.

59 D. Bröll, C. Kaul, A. Krämer, P. Krammer, T. Richter, M. Jung, H.Vogel, and P. Zehner, *Angew. Chem.* 1999, **111**, 3180; *Angew. Chem. Int. Ed.,* 1999, **38**, 2998.

60 A. S. Barnard and A. L. Curtiss, *Nano Lett.*, 2005, **5**, 1261.

61 Y. Wang, L. Zhang, K. Deng, X. Chen, and Z. Zou, *J. Phys. Chem. C* 2007, **111**, 2709.

62 U. Müller, J. Siekmann, und G. Frenzen, *Acta Cryst*., 1996, **C52**, 330.

63 R. Sai, Y. Lu, T. Lunkenbein, N. Miyajima, L.-T. Yan, M. Ballauf, and J. Breu, *Small*, 2009, **5**, 1326.

64 M. Müllner, T. Lunkenbein, N. Miyajima, J. Breu, and A. H. E. Müller, *Small*, 2012, **8**, 2636.

65 M. N. Tahir, P. Theato, P. Oberle, G. Melnyk, U. Kolb, M. Stepputat, and W. Tremel, *Langmuir*, 2006, **22**, 5209.

66 M. N. Tahir, M. Eberhardt, P. Theato, S. Faiß, A. Janshoff, T. Gorelik, U. Kolb, W. Tremel, *Angew. Chem.*, 2006, **118**, 922; *Angew. Chem. Int. Ed.*, 2006, **45**, 908.

67 H. Schäfer, *Angew. Chem.*, 1971, **83**, 35; *Angew. Chem. Int. Ed. Engl*., 1971, **10**, 43.

68 M. Binnewies, R. Glaum, M. Schmidt, P. Schmidt, *Chemische Transportreaktionen*, De Gruyter, Berlin, 2011.

Cite this: DOI: 10.1039/c0xx00000x

www.rsc.org/xxxxxx

ARTICLE TYPE

Synthesis of single crystalline sub-micron rutile TiO_2 rods using hydro-thermal treatment in acidic media

Patrick Leidich, Olga Linker, Martin Panthöfer, and Wolfgang Tremel*

Received (in XXX, XXX) Xth XXXXXXXXX 20XX, Accepted Xth XXXXXXXXX 20XX

DOI: 10.1039/b000000x

We describe the growth mechanism of single-crystalline rutile rods with tuneable size from fused titania.